Thin Solid Films 518 (2010) 1767–1773

Contents lists available at ScienceDirect

Thin Solid Films

journal homepage: www.elsevier.com/locate/tsf

Non-destructive evaluation of carrier transport properties in $CuInS_2$ and $CuInSe_2$ thin films using photothermal deflection technique

Anita R. Warrier, K.G. Deepa, Tina Sebastian, C. Sudha Kartha, K.P. Vijayakumar *

Department of Physics, Cochin University of Science and Technology, Cochin 682 022, India

ARTICLE INFO

Available online 19 September 2009

Keywords:
Photothermal
Thinfilm
Mobility
Carrier lifetime
Surface recombination velocity

ABSTRACT

Photothermal deflection technique (PTD) is a non-destructive tool for measuring the temperature distribution in and around a sample, due to various non-radiative decay processes occurring within the material. This tool was used to measure the carrier transport properties of $CuInS_2$ and $CuInSe_2$ thin films. Films with thickness <1 µm were prepared with different Cu/In ratios to vary the electrical properties. The surface recombination velocity was least for Cu-rich films (5×10^5 cm/s for $CuInS_2$, 1×10^3 cm/s for $CuInSe_2$), while stoichiometric films exhibited high mobility (0.6 cm^2/V s for $CuInS_2$, 32 cm^2/V s for $CuInSe_2$) and high minority carrier lifetime (0.35 µs for $CuInS_2$, 12 µs for $CuInSe_2$).

© 2009 Elsevier B.V. All rights reserved.

1. Introduction

In terms of cost and efficiency, thin film solar cells hold an optimistic fervour as future resource for sustainable energy. Commercial Cu (In,Ga)(Se,S)$_2$ (CIGS) modules have also entered the market (Siemens Solar shipped 300 kWp in 1999, Maycock, 2000) with top efficiencies of over 11% [1]. It is believed that CIGS together with CdTe will conquer the market share on price and the use of relatively simple production technologies. $CuInS_2$, having a band gap of 1.53 eV is considered to be an ideal material for photovoltaic application [2]. The difficulties in controlling the sulfur during deposition and the reported rapid diffusion of metals and impurity species, even at low temperatures, slow down the development of this material. However, devices with 11.4% efficiency have been reported [3]. On the other hand, $CuInSe_2$, with a band gap of 1 eV, has proved to be a leading candidate for photovoltaic applications. It is one of the most absorbing semiconductor materials (absorption coefficient of 3–6$\times10^5$/cm) and also makes an excellent junction and solar cell [4]. $CuInSe_2$ films are as good an electronic material as its single-crystal counterpart. This makes $CuInSe_2$ based solar cells less sensitive to impurities, grain size and crystalline defects. Devices with active area efficiency of 15.4% have been fabricated from $CuInSe_2$ [5]. However, the performance of the solar device critically depends upon the quality of surface of the absorber, due to the fact that in $CuInS_2$ (Se_2)-based cells most of the photons are absorbed close to the surface. Moreover, the presence of crystalline defects or secondary phases may lead to a reduction of lifetime of the photogenerated carriers, therefore affecting the cell performance. In this sense, stoichiometric conditions and substrate temperature during the formation of the absorber have been found to directly influence the physico-chemical characteristics of the resultant material, which in turn, determine its optoelectronic behavior. Surface condition of a thin slice of semiconductor material can affect profoundly the electrical properties of the slice, in particular, those characteristics depending on the minority carrier lifetime and electrical conductivity. Surface recombination velocity (SRV) which is a measure of rate of recombination between electrons and holes at the surface of semiconductors, is a significant parameter in characterizing surface property of solar cell materials. This also describes directly the recombination rate of the excess carriers via the surface electronic states and is determined mainly by the surface imperfection and contamination. Higher SRV at the front surface of a semiconductor solar cell will lead to higher surface losses of excess photo carriers and inversely affects the photo response. This greatly depends on the growth condition as well as on the polishness of the surface. Minority carrier lifetime (τ) in semiconductors is defined as the average time it takes for the excess minority carriers to recombine. Recombination activity increases proportionally to defect density and hence lifetime measurements give an estimate of the defect concentration as well. Unintentional lattice defects in semiconductors affect the minority carrier lifetime. These lattice defects and surface defects, which are formed during film growth, lead to scattering of carriers, which in turn affect the material's carrier diffusion coefficient and hence their mobility (μ). Knowledge of these properties and their variation with preparatory condition is essential for fabrication of a good solar cell material, as they have high impact on the short circuit current and open circuit voltage of solar cells. Thus the determination of SRV, τ, and μ is vital for achieving better material for solar cell design with higher efficiencies. The knowledge of their variation with thin film deposition conditions would allow us to optimise the fabrication parameters.

Photoconductance decay [6], surface photo voltage [7], photoluminescence [8], transient microwave reflectance technique [9] and

* Corresponding author. Tel.: +91 484 257 7103; fax: +91 484 257 7595.
E-mail address: kpv@cusat.ac.in (K.P. Vijayakumar).

0040-6090/$ – see front matter © 2009 Elsevier B.V. All rights reserved.
doi:10.1016/j.tsf.2009.09.029

quasi steady state photo conductance [10] are widely used for characterizing the minority carrier lifetime and diffusion length. Although the number of methods for evaluating SRV and minority carrier lifetime has been reported, specific environment conditions and complex techniques are required in all these methods, which limit the wide application of these techniques. Photothermal deflection technique (PTD) is a relatively simple and non-destructive technique for the measurement of SRV, minority carrier lifetime and mobility. This technique deals with the detection of heat generated by the sample, due to non-radiative deexcitation processes, following the absorption of light. Photothermal signal depends not only on the optical and thermal properties but also on electronic transport characteristics of semiconductor materials like minority carrier lifetime, carrier diffusion length and the surface recombination velocity. Photothermal techniques were developed for the characterization of materials, biological samples [11], thin films [12], imaging of subsurface defects [13] in metal lines and characterization of solar selective surfaces [14]. These techniques are becoming valuable tools for analysing semiconductor materials especially in manufacturing electronic devices [15].

1.1. Photothermal deflection technique

Photothermal effect occurs when thermal waves are generated due to periodic heating of the material, illuminated by periodically chopped light source. In the present work, we used transverse PTD technique, in its skimming configuration, to characterize the thermal and electronic transport properties of p-type $CuInS_2$ and $CuInSe_2$ thin films. Here, the thin film under investigation is illuminated with a periodically chopped optical beam, focused to a small spot size of diameter 100 µm on the surface; this induces thermal waves that diffuse into the sample and surrounding medium, producing a temporally varying gradient of the refractive index, which can deflect a probe beam from its initial trajectory. PTD technique, when applied in its transverse configuration with probe beam travelling at some fixed height from the sample surface, offers a useful way to investigate semiconductor samples [16]. It is a powerful tool for the evaluation of non-radiative states in semiconductors, since the PT signal amplitude is directly related to the amount of light, absorbed and converted by the sample into thermal waves, through non-radiative processes. Further in semiconductors, it is the presence of defects and impurities that contribute to the non-radiative nature of the material. Fournier et al. had put forth a theoretical model for investigating the transport properties of silicon wafers [17]. We employed this model for determining the carrier mobility of the carriers successfully but the theory was futile when it was applied for determination of SRV and τ. Hence a one-dimensional theoretical model was developed taking into consideration our experimental limitations and properties of sample under investigation.

2. Theoretical background

A one-dimensional model, which predicts the photothermal amplitude, was developed for determining the thermal and electronic transport properties of semiconductor thin films. Here we assumed that optical absorption takes place throughout the sample thickness and the electronic diffusion length of the sample is less than the spot size of the incident beam. The semiconductor material is excited using a monochromatic beam whose intensity is modulated periodically with frequency $\omega = 2\pi\upsilon$, where υ is the modulation frequency. The flux of photons penetrating into depth z of the sample is given by,

$$I = \frac{I_0}{2} e^{-\beta z} \mathrm{Re}[1 + e^{i\omega t}] \tag{1}$$

where I_0 is the intensity (W/m^2) of the incident light and β is the optical absorption coefficient (m^{-1}) of the photo excited semiconductor material at the excitation wavelength. The material absorbing this radiation would release thermal waves, which in turn, heat up the fluid around the material, thus producing a refractive index gradient in the fluid. The refractive index gradient produced in the medium due to heat diffused from the sample is given by,

$$\frac{dn}{dt} = \frac{dn}{dt}\frac{dT(z,t)}{dz} \tag{2}$$

where n is the refractive index of the fluid and dn/dt is the temperature coefficient of refractive index (K^{-1}). When another beam is passing through this medium, its path will be deflected. The angular deflection of the probe beam path is given by,

$$\theta \propto \frac{1}{n}\frac{\partial n}{\partial T}\frac{\partial T(z,t)}{\partial z} \tag{3}$$

Here $\frac{\partial T(z,t)}{\partial z}$ is the temperature gradient, produced in the fluid in the direction perpendicular to the propagation of the probe beam. In order to determine the deflection, it is necessary to determine thermal contribution due to the three different processes: immediate thermalization of carriers to band gap, non-radiative bulk recombination and non-radiative surface recombination. Fournier et al. have reported such analysis earlier. According to this model, mobility of the sample can be determined from the slope of variation of Log_e (signal amplitude) with (chopping frequency)$^{1/2}$ [17]. We have extended this model to transverse photothermal deflection in skimming configuration where the probe is propagating through a fluid medium, simply surfing the sample surface, in order to study thermal and electronic transport properties of semiconductor thin films.

2.1. Minority carrier diffusion equation

When the sample is irradiated with a beam of energy greater than the band gap it results in the excitation of carriers from valence band to conduction band. The number of excess carriers thus generated in the material can be determined by solving the minority carrier diffusion equation, which is given by,

$$D\frac{\partial^2 N(z,t)}{\partial z^2} - \frac{\partial N(z,t)}{\partial t} - \frac{\Delta N}{\tau} + G(z,t) = 0 \tag{4}$$

where,

D	electronic carrier diffusion coefficient (cm^2/s)
N	number of minority carriers (cm^{-3})
τ	minority carrier lifetime (s)
G	$\frac{I_0}{2E}e^{-\beta z}$
E	Energy $h\nu$ of the incident photon

To calculate the concentration of excess carriers generated in the semiconductor thin film, we make the following assumptions,

1. The material is in steady state and the carrier concentration does not vary with time, the term $\frac{\partial N(z,t)}{\partial t}$ vanishes.
2. The sample being optically transparent (penetration depth $\mu_b > l$) and thermally thick (thermal diffusion length $\mu_s > l$) light penetrates throughout the thickness of the sample and excess carriers are generated throughout the film thickness (l) (Fig. 1). Hence there is no diffusion along the direction of propagation (z) of the beam, making $\frac{\partial^2 N}{\partial z^2} = 0$.

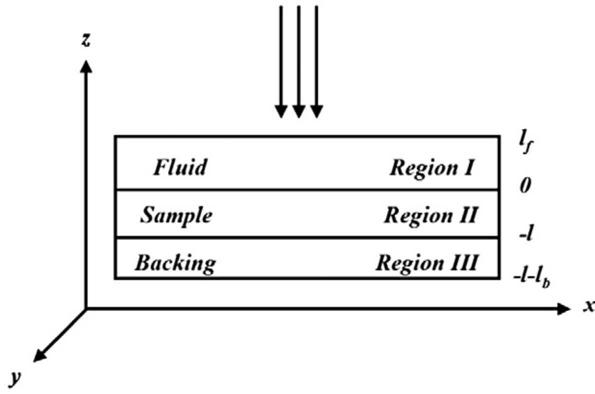

Fig. 1. Sample geometry of PTD technique.

Hence the minority carrier diffusion equation may be written as,

$$N[z] = \frac{\beta I_0}{2E}\tau e^{-\beta z} \tag{5}$$

2.2. Heat diffusion equation

Thermal distribution in and around the sample due to light absorption is determined by solving the heat diffusion equations. Here we assume that only the film coated over the substrate is acting as the thermal source. The geometry of the fluid, sample, and substrate is shown in Fig. 1. The heat diffusion equation in the three regions: fluid, sample and backing is given by,

$$\frac{\partial^2 T_f(z,t)}{\partial z^2} = \frac{1}{D_f}\frac{\partial T_f(z,t)}{\partial t} \text{ Region I} \tag{6a}$$

$$\frac{\partial^2 T_s(z,t)}{\partial z^2} = \frac{1}{D_s}\frac{\partial T_s(z,t)}{\partial t} - \frac{\beta I_0}{2k_s}\frac{E-E_g}{E}e^{-\beta z} - \frac{E_g}{k_s\tau}N[z] \text{ Region II} \tag{6b}$$

$$\frac{\partial^2 T_b(z,t)}{\partial z^2} = \frac{1}{D_b}\frac{\partial T_b(z,t)}{\partial t} \text{ Region III} \tag{6c}$$

In Eq. (6b) the 2nd term is due to the non-radiative intraband thermalization process by which excited carriers relax to the bottom of the conduction band with the release of energy to lattice. The 3rd term is due to non-radiative recombinations happening in the bulk of the material due to the presence of traps and recombination centres. The boundary conditions given in Eqs. (7a), (7b), (7c), (8a), and (8b) indicate that the temperature distribution must be equal at the region boundaries and the heat continuity equation, which states that heat flowing out of one region must be equal to heat flowing into the adjoining region, must be obeyed,

$$T_f(z,t)_{(z=0)} = T_s(z,t)_{(z=0)} \tag{7a}$$

$$T_s(z,t)_{(z=-l)} = T_b(z,t)_{(z=-l)} \tag{7b}$$

$$T_f(z,t)_{(z=l_f)} = T_b(z,t)_{(z=-(l-l_b))} = 0 \tag{7c}$$

$$k_f\frac{\partial T_f(z,t)}{\partial z}_{(z=0)} = k_s\frac{\partial T_s(z,t)}{\partial z} sN[0]E_{g(z=0)} \tag{8a}$$

$$k_s\frac{\partial T_s(z,t)}{\partial z}_{(z=-l)} = k_b\frac{\partial T_b(z,t)}{\partial z}_{(z=-l)} \tag{8b}$$

With the assumption that l_f and l_b are larger than the distances up to which periodic heat pulse diffuses the boundary condition is applied only to the sample–fluid and sample–backing interface. Here, D_i is the diffusivity (cm^2/s); k_i is the thermal conductivity (W/cm °C). With k_i representing the fluid medium, sample and backing, s is the surface recombination velocity. Solving the above heat diffusions equations, the complex amplitude of modulated temperature $T(z, t)$ in the three regions is given by,

$$T_f(z) = T_s e^{-\sigma_f z} \tag{9a}$$

$$T_s(z) = C_1 e^{\sigma_s z} + C_2 e^{-\sigma_s z} - (C_3 + C_4)e^{-\beta z} \tag{9b}$$

$$T_b(z) = W e^{\sigma_b (z+l)} \tag{9c}$$

where

$$C_3 = \frac{\alpha I_0}{2k_s}\frac{E-E_g}{E}e^{-\beta z}$$
$$C_4 = \frac{E_g}{k_s\tau}\frac{\alpha I_0}{2E}e^{-\beta z}$$
$$\sigma_i = \sqrt{\frac{i\omega}{D_i}}$$

The coefficients C_1, C_2, T_s and W are determined by using the boundary conditions (Eqs. (7a), (7b), (7c), (8a), and (8b)). The temperature distribution at the sample surface due to thermal waves generated from the sample is given by,

$$T_s = \left\{ \frac{\left[\sqrt{D_f D_s}\left(-V_1 B\sigma_b^2 D_b^{\frac{3}{2}} k_s + V_2 D_s\left\{\begin{array}{l}\beta\sqrt{D_s k_b}\langle B\beta + Ck_s\rangle - \\ \sigma_s\langle B\sigma_b\sqrt{D_b k_b} - C\sqrt{D_b k_s^2}\rangle\end{array}\right\}\right) + D_s k_s\left(V_3 C\left\{\sigma_s\sqrt{D_s k_b} + k_s\beta\sqrt{D_b}\right\} + V_1 B\beta^2\sqrt{D_b}\right)\right]}{\left[\sqrt{i\omega}(i\omega - \beta^2 D_s)\left(\begin{array}{l}V_2\left\{D_s k_b k_f + \sqrt{D_b D_f}k_s^2\right\} + \\ V_1\left\{\sqrt{D_s k_s}\langle\sqrt{D_f K_b} + \sqrt{D_b k_f}\rangle\right\}\end{array}\right)\right]} \right\} \tag{10}$$

where

$$V_1 = 1 + e^{2l\sigma_s}$$
$$V_2 = -1 + e^{2l\sigma_s}$$
$$V_3 = V_1 - 2e^{l(\beta+\sigma_s)}$$
$$B = sN(0)E_g$$
$$C = C_3 + C_4$$

The temperature gradient around the sample causes refractive index variation in the fluid as shown in Eq. (2). Probe beam deflection amplitude is determined by using Eq. (10) in Eq. (2). By solving this we get the theoretical value of the beam deflection or signal amplitude. A theoretical plot, showing the variation of signal amplitude with chopping frequency, is obtained using MATHEMATICA 5.1. A fit between the experimental and theoretical plot is obtained by using the unknown parameters as adjustable fit parameters. The best fit thus obtained can reveal the material parameters. This method was used for determining the surface recombination velocity and minority carrier lifetime of $CuInS_2$ and $CuInSe_2$ thin films.

3. Experimental details

3.1. Deposition of $CuInS_2$ thin films

$CuInS_2$ thin films were deposited using aqueous solutions of $CuCl_2$, $InCl_3$ and thiourea using chemical spray pyrolysis (CSP) method on micro glass slides. Cleaned glass slides were placed on a base plate with heater rods embedded in it to facilitate uniform heating. The substrate temperature was maintained with the help of a feedback

circuit that controlled the heat supply. Temperature of the substrate can be varied from room temperature to 732 K. Spray head and heater with the substrate were kept inside a chamber provided with an exhaust fan for removing gaseous byproducts and vapour of the solvent. During spray, temperature of substrate was kept constant with an accuracy of ± 5 K. The carrier gas and the solution were fed into the spray nozzle at predetermined constant pressure and flow rate. In this work, $CuInS_2$ thin film samples of size 3×3 cm were prepared by taking three Cu/In ratios 0.5, 1.0 and 1.5 and the samples were coded as CIS1, CIS2, CIS3 respectively. Flow rate was kept constant at 1 ml/min, while spray volume was 30 ml and substrate temperature was 300 °C. The films had band gap of 1.3 eV and thickness of 0.58, 0.46 and 0.26 µm for CIS1, CIS2 and CIS3 respectively.

3.2. Deposition of $CuInSe_2$ films

$CuInSe_2$ thin films were deposited through sequential evaporation of selenium, indium and copper, at moderately low substrate temperature, as an alternative to high temperature deposition of the elements or compound evaporation. Structure of the film was Glass/In/Se/Cu. Indium was evaporated at 100 °C; selenium at 50 °C and copper at room temperature and this layer was annealed at 400 °C. All these processes were carried out at a pressure of 2×10^{-5} mbar. And the samples were coded according to the Cu/In ratios 0.2, 0.25 and 0.3 as CISE1, CISE2 and CISE3. The films had a band gap value of 1.2 eV and a thickness of 0.5 µm.

3.3. Photothermal beam deflection set up

The experimental set up used for the characterization is shown in Fig. 2. He–Ne laser (632 nm, 10 mW) was used as the excitation beam (pump beam). The incident beam was modulated using a mechanical chopper (Stanford SR540) with frequency range from 4 Hz to 4 KHz. Another beam (probe beam) of wavelength 546 nm and power 1 mW was placed perpendicular to the pump beam and allowed to grace the sample surface (Fig. 2). Deflection of the probe beam path was detected using a Bi-cell position sensitive detector (PSD) and the signal was measured using a lock in amplifier (SR 830 DSP). The sample was mounted on the sample cell filled with coupling fluid (medium). The medium used in this experiment was carbon tetrachloride, since its thermal diffusivity is very low and temperature coefficient of refractive index gradient is very high (5×10^{-4}/K). This would facilitate the amplification of deflected signal. This set up was automated and interfaced to computer by RS232 and the data acquisition and analysis is done using Labview 7.1.

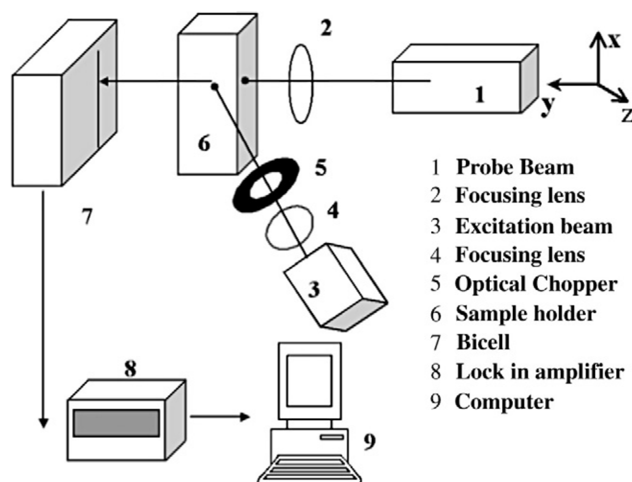

Fig. 2. Schematic sketch of transverse PTD experimental set up in skimming configuration.

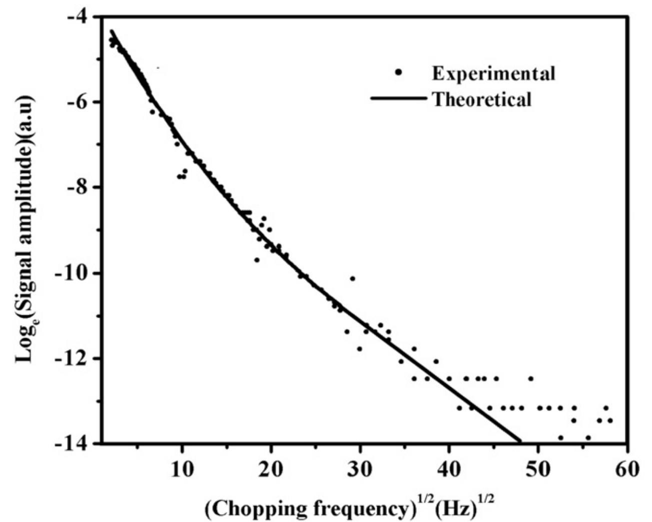

Fig. 3. Plot of Log$_e$ (signal amplitude) versus (chopping frequency)$^{1/2}$ for p-type silicon wafer.

4. Results and discussion

Determining the transport properties of p-type silicon wafer proved the reliability of the technique and theory. Silicon wafer had a thickness of 300 µm and an absorption coefficient of 3×10^3 cm^{-1} (632 nm), hence the entire incident light is absorbed within 3 µm and the thickness of backing is taken as $(l-3)$ µm. Fig. 3 shows the experimental and theoretical plot of Log$_e$ (signal) versus (chopper frequency)$^{1/2}$ with fit for p-type Si wafer. The transport parameters' thermal diffusivity, minority carrier lifetime and surface recombination velocity were obtained as variable fit parameters. There is good agreement between experimental and theoretical plots. Table 1 shows the parameters used for fitting the experimental plot with theoretical calculations and matches well with reported values [17]. The method for determining the minority carrier mobility was proved by performing the experiment on ZnO thin films [18]. The mobility was 17.1 cm^2/Vs, matching with earlier reported values [19]. The $CuInS_2$ and $CuInSe_2$ thin films were irradiated using the intensity-modulated beam and the resulting deflection of probe beam is detected using Bi-cell PSD. The plot of Log$_e$ (signal) versus (chopper frequency)$^{1/2}$ for $CuInS_2$ and $CuInSe_2$ thin films (Figs. 4 and 5) prepared by varying the Cu/In ratio shows the variation of amplitude of signal with modulation frequency. Fig. 4 shows the plot of Log$_e$ (signal amplitude) versus (chopper frequency)$^{1/2}$ for Cu-rich (CIS1), stoichiometric (CIS2) and Cu-poor (CIS3) $CuInS_2$ samples. The nature of variation of the signal with frequency is such that it decreases with increase in chopper frequency and this variation largely depends on the composition and surface morphology of the film.

Table 1
Parameters used for theoretical fitting of p-type Si wafer.

Fit parameters	Code	Unit	Fit value
Thermal diffusivity of sample	α_s	m^2/s	0.92×10^{-4}
Thermal diffusivity of fluid	α_f	m^2/s	7.5×10^{-8}
Thermal diffusivity of backing	α_b	m^2/s	0.92×10^{-8}
Thickness	l	m	300 µm
Thermal conductivity of sample	k_s	W/m K	131
Thermal conductivity of fluid	k_f	W/m K	0.104
Thermal conductivity of backing	k_b	W/m K	131
Intensity of incident beam	I_0	W/m^2	100
Absorption coefficient of sample	β	m^{-1}	3×10^3
Band gap energy of sample	E_g	eV	1.1
Wavelength of incident beam	λ	m	632×10^{-9}
Minority carrier lifetime	τ	µs	30
Surface recombination velocity	s	m/s	1

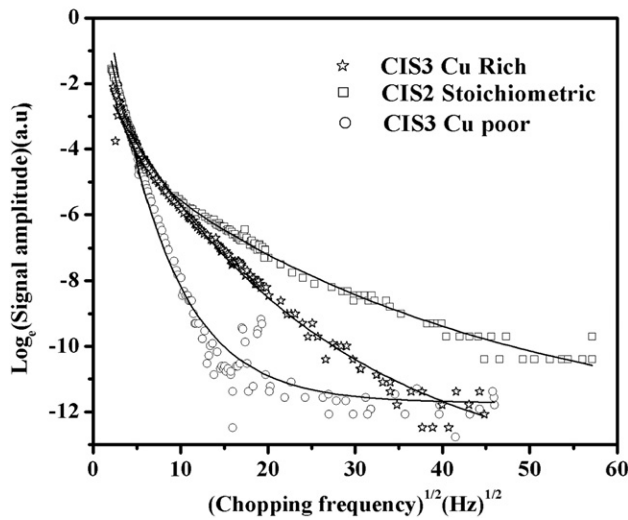

Fig. 4. Plot of Log$_e$ (signal amplitude) versus (chopping frequency)$^{1/2}$ for $CuInS_2$ thin films CIS1, CIS2, CIS3.

It is observed that for Cu-poor samples, the signal was comparatively low, which implied that the thermal contribution due to non-radiative recombinations was least here. Also the variation of the signal with frequency was rapid in low frequency regime (<200 Hz) and shows a "peak" nature in the frequency range (225 to 400 Hz). After this it remains almost constant in the higher frequency region (>400 Hz). For Cu-rich films, the signal was higher in low frequency region and so for these samples the non-radiative thermal contribution was naturally higher. But in high frequency region, the signal variation showed a "rapid decrease" with increase in frequency. Hence the thermal contribution in CIS1 was dominated by intraband thermalization of carriers while for CIS2 and CIS3 the thermal contribution in low frequency region was almost twice due to contribution from non-radiative bulk recombination. The EDAX results of these samples showing the composition (%) of Cu, In, and S are shown in Table 2. Thus the formation of defects in the bulk is comparatively low in Cu-poor samples. The transport properties of CIS1, CIS2 and CIS3 can be determined as "variable fit parameters" from the fit between theoretical and experimental plot. Table 3 shows the values of mobility, SRV and minority carrier lifetime obtained from the theoretical fit and we find that the mobility and minority carrier lifetime were high for stoichiometric films. For Cu-rich films, the SRV

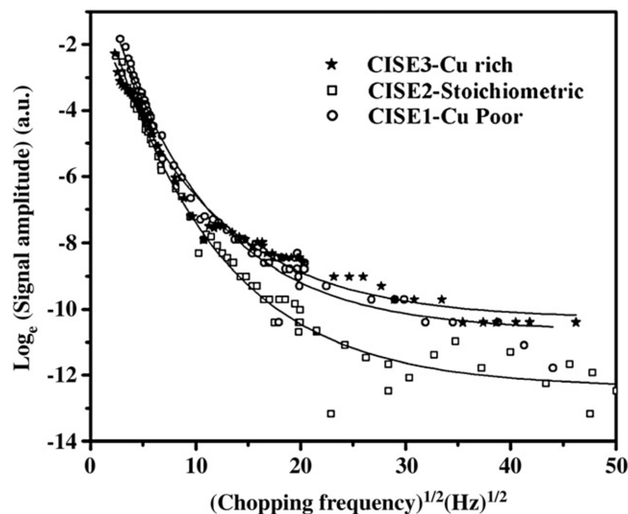

Fig. 5. Plot of Log$_e$ (signal amplitude) versus (chopping frequency)$^{1/2}$ for $CuInSe_2$ thin films CISE1, CISE2, CISE3.

Table 2
EDAX data of $CuInS_2$ thin films CIS1, CIS2, CIS3.

Code	Cu%	In%	S%	Cl%
CIS1	14.8	30.25	47.8	7.15
CIS2	22.37	24.26	46.58	6.78
CIS3	28.3	22.85	48.8	0.05

Table 3
μ, τ, SRV of $CuInS_2$ thin films CIS1, CIS2, CIS3.

Code	Mobility (cm^2/V s)	τ (ns)	SRV (cm/s)
CIS1	0.23	10	1.3×10^{10}
CIS2	0.60	350	2×10^{8}
CIS3	0.21	1	5×10^{5}

is reduced by an order of 10^5. They were in good agreement with reported values [20,21]. Film surface quality was improved due to the crystallization mechanism induced by $Cu_{2-x}S$ phase. Cu deficiency in a sample surface can cause formation of complex defects in the surface. Also the crystalline quality of the film is affected in the Cu-poor samples while in Cu-rich film crystallinity is good with orientation along the 112 plane (Fig. 6). For Cu-poor films the conductivity is also generally very low, making it almost unsuitable as absorber layer. These results can be linked with AFM images (Fig. 7a and b). Here we observe that films prepared with excess Cu in the initial solutions have sharp edged surface while that of Cu-poor are irregular. This could be because Cu-rich starting solutions decrease the formation temperature of $CuInS_2$ films promoting recrystallization and crystal growth in films with well faceted and larger grains [22]. Though the surface quality of Cu-rich films is good, mobility and lifetime are better for stoichiometric films. Though excess of Cu promotes surface quality the bulk is packed with defects and there are deteriorating effects due to segregated $Cu_{2-x}S$ phases in the grain boundaries. Defects in the grain boundaries can cause scattering of carriers and affect their mobility by diminishing the diffusion coefficient. In Cu-poor films, deficiency of Cu is accommodated by the introduction of complex defects in the surface. The large number of surface states leads to high recombination rates at the surface, leading to high surface recombination velocities (~10^{10} cm/s). Hence when there is excess of Cu the SRV is restrained to 10^5 cm/s.

For $CuInSe_2$ films the non-radiative contribution is the least for stoichiometric samples (Fig. 5). For Cu-poor films the shallow acceptor level due to Cu vacancy (V_{Cu}) is assumed to be the main dopant (for Cu-rich films Cu in In antisites (Cu_{In}) forms a similar kind of defect) and Se vacancies (V_{se}) act as compensating donors as well as defects due to the creation of double donor Indium in Cu (In_{Cu})

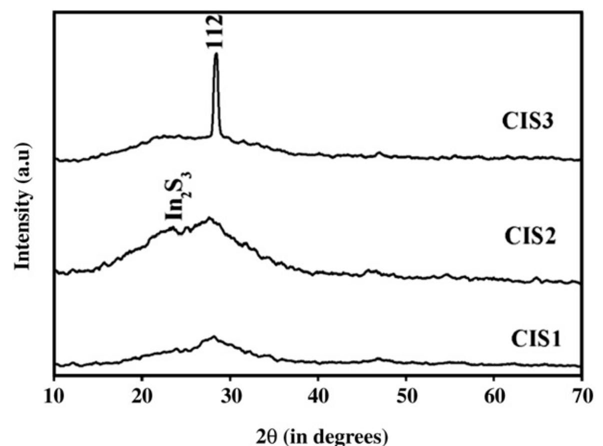

Fig. 6. XRD pattern of $CuInS_2$ thin films CIS1, CIS2, CIS3.

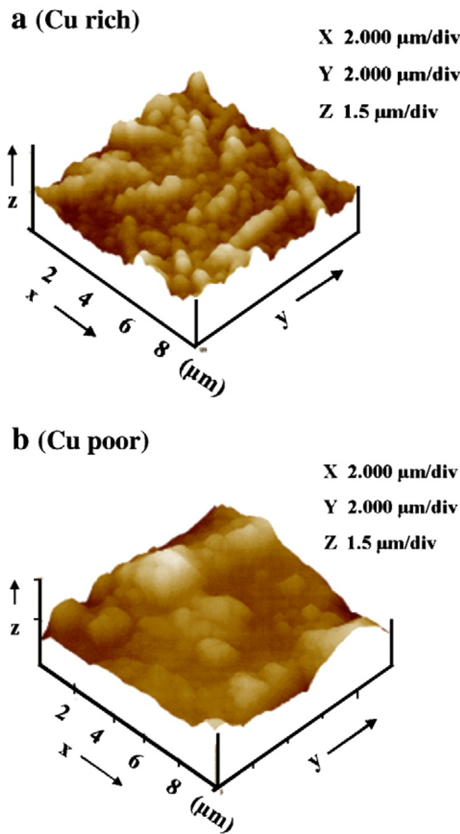

Fig. 7. AFM image of (a) Cu-rich and (b) Cu-poor $CuInS_2$ thin films.

vacancies. The surface states due to V_{Se} cause band bending in the film, which leads to liberation of Cu from its lattice sites and cause Cu migration towards the neutral part of the film. The remaining Cu vacancies (V_{Cu}) close to the surface result in high density of acceptor states or formation of p^+ defect layer at the film surface. This defect layer could be responsible for the high recombination velocity observed in Cu-poor films. The density of defects is generally reported to be lower for $CuInSe_2$ films with stoichiometric composition. This can be correlated to the improvement of mobility and minority lifetime for stoichiometric films. Similar to $CuInS_2$ films, for Cu-rich $CuInSe_2$ films the SRV decreased and was three times lesser (1000 cm^2/s) than the Cu-poor $CuInSe_2$ films (3000 cm^2/s). From AFM images (Fig. 8a and b), the surface is triangular and regular for Cu-rich films, while for Cu-poor films the surface is rather irregular and spherical. The atomic percentage of Cu, In and Se in the films CISE1, obtained from EDAX is shown in Table 4. In Cu-rich samples there is a reported presence of ($Cu_{2-y}Se$) phases, which was found to enhance the conductivity of the material. But in device form, films with excess Cu may not be useful due to the presence of secondary phases ($Cu_{2-y}Se$) preferentially at the surface of the film as the metallic nature of this phase affect formation efficient junction. We also observed that the minority carrier mobility and lifetime were suppressed due to excess Cu in the film. Table 5 shows the mobility, minority carrier lifetime and surface recombination velocity obtained for $CuInSe_2$ films. XRD pattern (Fig. 9) indicates that the crystalline quality of the stoichiometric film was better. The concentration of copper played a profound role in deciding surface quality of the film and stoichiometric films are required for obtaining films with high mobility and minority carrier lifetime.

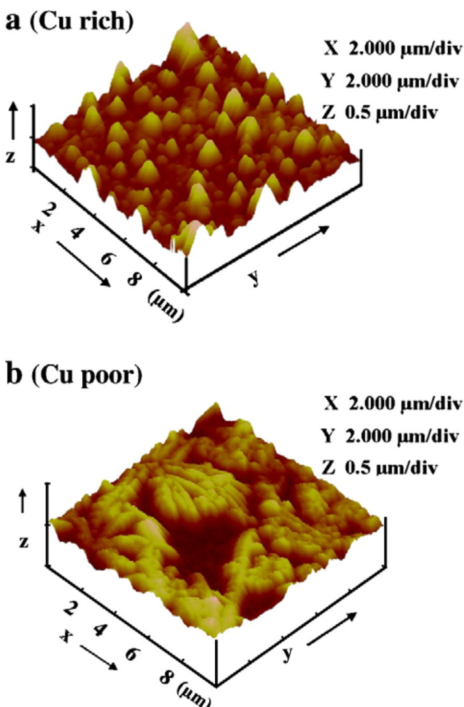

Fig. 8. AFM image of (a) Cu-rich and (b) Cu-poor $CuInSe_2$ thin films.

Table 4
EDAX data of $CuInSe_2$ thin films CISE1, CISE2, CISE3.

Code	Cu%	In%	S%
CISE1	19.75	20.21	60.04
CISE2	24.92	24.98	50.10
CISE3	22.84	20.19	56.97

Table 5
μ, τ, SRV of $CuInSe_2$ thin films CISE1, CISE2, CISE3.

Code	Mobility (cm^2/V s)	τ (µs)	SRV (cm/s)
CISE1	1.25	2	3000
CISE2	32	12	1500
CISE3	2.12	4	1000

5. Conclusions

The mobility (μ), minority carrier lifetime (τ) and surface recombination velocity (SRV) of silicon, $CuInS_2$ and $CuInSe_2$ films were determined by photothermal deflection technique. The values obtained for Si were compared with earlier reports and were found

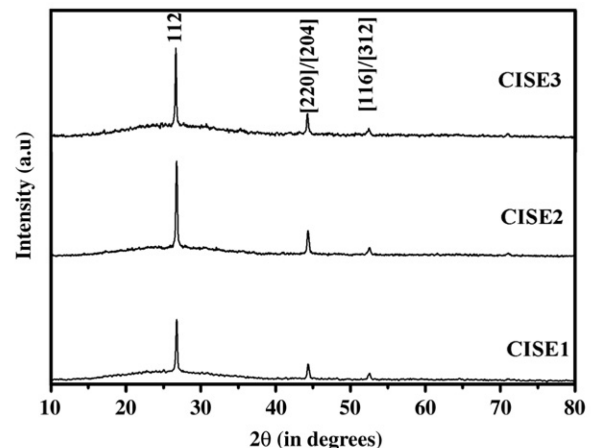

Fig. 9. XRD pattern of $CuInSe_2$ thin films CISE1, CISE2, CISE3.

to be more or less the same. This proved the reliability of the technique. The role of Cu in improving the surface quality of $CuInS_2$ and $CuInSe_2$ is apparent from the PTD studies. Excess Cu reduced the surface recombination velocity by an order of 10^5 in $CuInS_2$ and three times in $CuInSe_2$ thin films. The stoichiometric films of both $CuInS_2$ and $CuInSe_2$ showed comparatively better mobility and minority lifetime compared to Cu-rich and Cu-poor samples. Thus we were able to demonstrate the use of PTD for measuring the transport properties of semiconductor thin films.

References

[1] K.L. Chopra, P.D. Paulson, V. Dutta, Prog. Photovolt. Res. Appl. 12 (2004) 69.
[2] H.L. Hwang, C.L. Cheng, L.M. Liu, C.Y. Sun, Thin Solid Films 67 (1980) 83.
[3] D. Braunger, D. Hariskos, T. Walter, H.W. Schock, Sol. Energy Mater. Sol. Cells 40 (1996) 97.
[4] K. Siemer, J. Klaer, I. Luck, J. Bruns, R. Klenk, D. Braunig, Sol. Energy Mater. Sol. Cells 67 (1–4) (2001) 159.
[5] J. Hedstrom, H. Ohlsen, Proceedings of the 23rd IEEE Photovoltaic Specialists Conference; (1993), Louisville, KY, 10–14 May, 1993, p. 364.
[6] F.X. Chen, R.Q. Cui, L. Xu, F.Y. Meng, Z.X. Zhao, Z.B. Zhou, Semicond. Sci. Technol. 19 (2004) 959.
[7] Y. Yan, Appl. Phys. Lett.71 (3), 21(1997), 407.
[8] D. Baek, S. Rouvimov, B. Kim, T.C. Jo, Appl. Phys. Lett. 86 (2005) 112110.
[9] S. Bothra, S.D. Tyagi, S.K. Ghandi, J.M. Borrego, Proceedings of 23rd IEEE Photovoltaic Specialists Conference, 1990, p. 404.
[10] G. Kumaravelu, M.M. Alkaisi, A. Bittar, D. Macdonald, J. Zhao, Curr. Appl. Phys. 4 (2004) 108.
[11] R.R. Anderson, H. Beck, U. Bruggemman, W. Farinelli, S. Jacques, J.A. Parrish, Appl. Opt. 28 (1989) 2256.
[12] M. Nestoros, Y. Karmiotis, C. Christofides, J. Appl. Phys. 82 (1997) 6220.
[13] A. Rosencwaig, in: A. Mandelis (Ed.), Progress in Photothermal and Photoacoustic Science and Technology, Vol II: Non-Destructive Evaluation (NDE), Prentice Hall, Englewood Cliffs, NJ, 1994, p. 73.
[14] A. Othonos, M. Nestoros, D. Palmerio, C. Christofides, R.S. Bes, J.P. Traverse, Sol. Energy Mater. Sol. Cell 51 (1998) 171.
[15] P. Grunow, R. Schieck, J. Appl. Phys. 77 (1995) 2773.
[16] V.A. Sabilkov, V.B. Sandormirskii, Phys. Status Solidi B120 (1983) 471.
[17] D. Fournier, C. Bocarra, A. Skumanich, N.M. Amer, J. Appl. Phys. 59 (1986) (1986) 787.
[18] M. Paulraj, S. Ramkumar, K.P. Vijayakumar, C. Sudha Kartha, K.G.M. Nair, T.S. Radhakrishnan, Proceedings of World Renewable Energy Congress VII, Cologne, Germany, 2002.
[19] Y.W. Heo, S.J. Park, K. Ip, S.J. Pearton, D.P. Norton, Appl. Phys. Lett. 83 (2003) 112.
[20] S. Mora, N. Romeo, L. Tarricone, Solid State Commun. 29 (1979) 155.
[21] K. Djessas, G. Masse, M. Ibannaim, J. Electrochem. Soc. 147 (4) (2000) 1235.
[22] M. Krunks, V. Mikli, O. Bijakina, E. Mellikov, Appl. Surf. Sci. 142 (1999) 356.